INDUCED DRAG AND WINGLETS

by R. Eppler, Universität Stuttgart, Germany

Presented at the XXIV OSTIV Congress, Omarama, New Zealand (1995)

This paper is a short version of a paper given at the XXIVth OSTIV Congress in Omarama, New Zealand. The complete paper with all mathematical derivations will be published in Zeitschrift für Flugwissenschaften und Weltraumforschung (ZFW), approximately July, 1996. (1)

Abstract

A simple method is described which allows consideration of the most significant higher order term in the calculation of the induced drag of nonplanar wings. This is the induced lift due to the velocities that the lifting vortices induce on themselves. This induced lift does not change the induced drag. It is positive for positive dihedral and winglets above the wing tip and negative for negative dihedral and winglets below the wing tip. Experiments with small models clearly demonstrate this difference which is neglected in the classical theory. This shows that the higher order effects should be taken into account. The results of several parameter variations are presented.

1. Introduction

The induced drag is for all "heavier than air" flying vehicles a significant contribution to the total drag. It is the equivalent of the energy contained in the air masses which must for the momentum balance be accelerated downward by any lifting wing of finite span. The induced drag would be present even if the viscosity of the air were not. It is therefore generally assumed that the induced drag is independent of the viscous drag. The induced drag is always calculated for a nonviscous fluid.

To this day the induced drag is mostly calculated based on the classical lifting line theory of L. Prandtl (6), for example by means of the numerical procedure of H. Multhopp (4). But already M. Munk (5) in his famous dissertation mentioned some effects like rollup of the vortex wake and induced lift which are neglected by the lifting line theory and should be regarded in more precise investigations. This has not been done (or forgotten) until recently when S. Schmid-Göller (7) "rediscovered" the induced lift without explicitly calculating it. The present paper mainly deals with the induced lift and shows that it is closely connected with the effect of the wake rollup.

2. Fundamentals

Any theory of induced forces on a wing must regard the following facts:

a). a nonviscous flow which was once irrotational re-

mains irrotational. An irrotational flow is a potential flow.

b). A vortex in a nonviscous flow can never end or begin or change its strength or circulation. A vortex with variable circulation must be understood as a variety of vortices which join or leave each other. This is the Helmholtz Law.

c). A single straight vortex of infinite length cannot be present without a total flow field in which all streamlines are circles with the vortex as axis, and the flow velocity w is

$$w = \frac{\Gamma}{2\pi r} \tag{1}$$

where Γ is the circulation of the vortex and r the radius of the streamline circle. It is also said that the vortex "induces" the velocity w.

d) A cambered vortec of variable strength which can according to b) not exist without other vortices joining or leaving it, induces also a velocity $\vec{w}$. It must be imaged that each very short element $\vec{g}$ of such a vortex induces at a point P a velocity again tangential to the circle whose axis is defined by $\vec{g}$. This is sketched in Figure 2.1. The total velocity that the vortex of the length S induces at P is the sum (integral) of the velocities that are induced by all elements of the vortex. This means, written in vector formulation

$$\vec{w} = -\frac{1}{4\pi}\int_0^S \Gamma(s)\frac{\vec{r}}{r^3} \times \vec{ds} \qquad (r = |\vec{r}|) \tag{2}$$

This is the well-known formula of Biot-Savart.

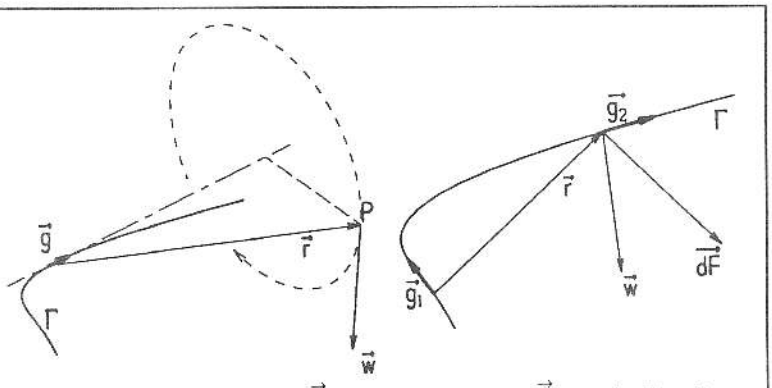

FIGURE 2.1 Induced velocity $\vec{w}$ of a vortex element $\vec{g}$ from the Biot-Savart equation. Element $\vec{dF}$ of the self-induced force.

e) A straight "bound" vortex of infinite length and the constant circulation Γ in a parallel flow of the velocity v_∞ experiences a force (lift) per unit length of

$$F = \rho v_\infty \Gamma \tag{3}$$

which is perpendicular to v_∞, and Γ. The direction is towards that side where the induced velocity has the same direction as v_∞. The force of a cambered vortex with variable Γ in a general flow field v must again be summarized over the forces on the elements $\vec{g} = \Gamma\vec{ds}$ which are

$$\vec{dF} = \rho\vec{v} \times \vec{q} \tag{4}$$

The flow field v may consist of the velocities being induced by the vortex itself. This case is sketched in Figure 2.1.

f) For vortex elements of a cambered vortex which are very close, the denominator r^3 in equation (2) is very small. This means, mathematically that a cambered vortex of finite strength undergoes an infinite force! This does not contradict nature. Single vortices of finite strength do not exist in nature. They would also contain infinite energy. These facts show that mathematical models of flows which contain isolated vortices of finite strength must be considered very carefully.

g) A finite vortex strength can be distributed on a vorticity surface, on which the vorticity is $\vec{\gamma}$. A vortex element is then

$$\vec{g} = \vec{\gamma}dA \tag{5}$$

where dA is a surface element, see Figure 2.2. It can be shown that in this case the induced velocities are finite everywhere except at the edge of the vortex surface, and the forces which the vorticity surface induces on itself are also finite.

The lifting-line theory models the wing as a single vortex with variable finite strength. The figure of Prandtl (6) is copied in Figure 2.3. The vorticity surface which must be present due to the variable Γ forms the wake. Their vortex lines are parallel to v_∞. The lifting vortex is straight in this case. No induced lift is present. This theory was and is extremely successful. Once it is used for nonplanar wings it must be considered very carefully because the lifting vortex would produce an infinite force. The same is true if the lifting vortex is swept forward or back.

Of course, this infinite force is not present on the real wing which does not consist of a single vortex. But there are forces due to the velocities that are induced from the wing at points of itself. The present paper is an at-

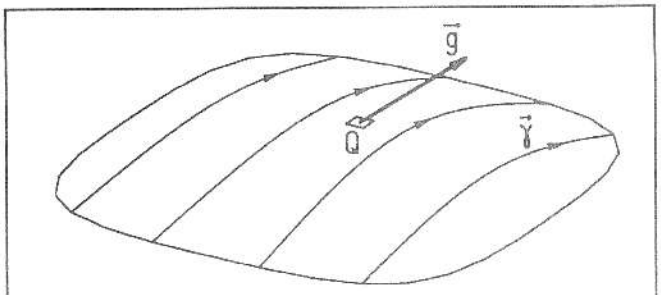

FIGURE 2.2 Vorticity distribution on a surface and vortex element of it.

tempt to calculate these forces.

3. Calculation of the Induced Forces

In the past 20 years several so called panel methods have been developed which permit comparison of the flow around very complex bodies like a complete aircraft with wing, fuselage, tail and engines. These methods subdivide the surface of the body into very many panels. On each panel a singularity distribution with unknown parameters is assumed. The singularities may be vorticities, doublets or sources. For lifting bodies a vortex wake must be added to satisfy the Helmholtz law. VSAERO (3) is an example of such a panel program. Such programs calculate the induced velocities from all panels and the wake to all panels. The flow conditions require that the induced flow together with the infinite flow must on each panel be tangential to the surface. This yields a linear equation system for the unknown parameters of the singularity distributions of the panels. Its solution describes the flow. The forces on the body can be calculated by summarizing the forces on all panels.

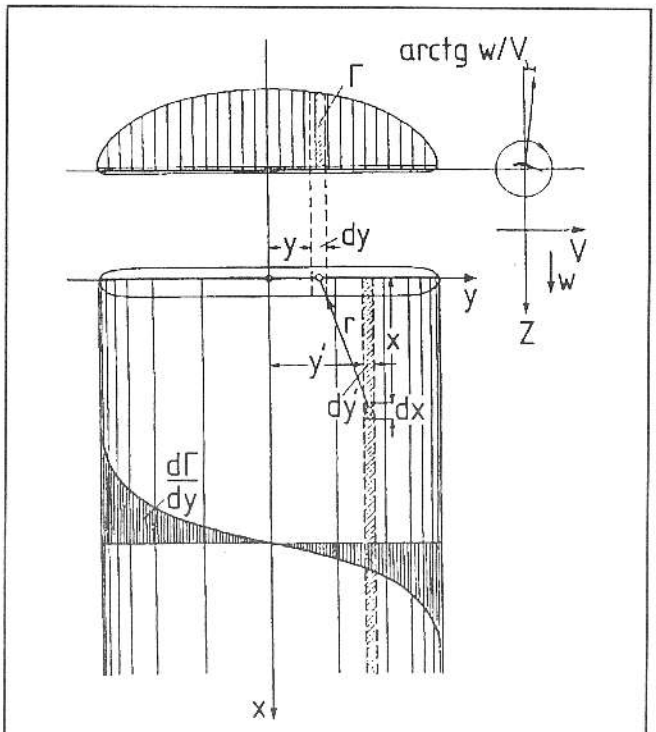

FIGURE 2.3 Classical lifting line Theory, *Prandtl*, 1918.

The panel methods consider all velocities which are induced by all panels. The summarized pressure forces of all panels thus include also the induced drag and the induced lift. A wing without fuselage and tail seems to be a simple problem for a panel method which even allows iterative cirrection of the shape of the wake to the local flow. Indeed, the pressure distributions from the panel methods look very good. But it turns out that the induced forces are mostly not computed precisely enough. They consist of small components of large forces. An example is a paper of VanDam (9) which was discussed by Smith and Kroo (8). Even with a very large number of panels the results were not reliable.

Another method calculates the forces in the Trefftz-plane far behind the wing. If a rigid wake is assumed lift and drag can be calculated in a very simple way in the Trefftz plane. S. Schmid Göller (7) showed that the induced drag is calculated correctly this way, but the lift from the Trefftz-plane does not contain the induced lift. In detail, he showed that in the Trefftzplane all forces are calculated which effect the total system in front of the Trefftz plane. This includes the forces on the wing and the wake.

$$F_{Trefftz} = F_{wing} + F_{wake} \qquad (6)$$

There are no drag forces on the wake because the wake vortices are parallel to v_∞ and all forces on them are perpendicular to them. But there are lift forces on the wake vortices once there are induced velocities in the spanwise direction. Such velocities are present once the wing is not planar, only the forces on planar wings are calculated correctly in the Trefftz plane.

The present paper uses the Trefftz plane also for nonplanar wings. But it additionally calculates the lift on the wake which must according to equation (6) be subtracted from the lift as evaluated in the Trefftz plane. There is a nice simplification in this approach. It could be shown that two parallel vortex elements induce on each other two forces which together are exactly zero. All vortex elements of the rigid wake are parallel to v_∞. The sum of all forces which are induced from the wake to itself thus vanish exactly. Only the forces due to induced velocities from the wing to the wake must be considered. Of course, if a nonplanar wing is modeled by a single vortex, these forces are again infinite, because they contain the induced lift which is infinite. This can be checked in detail. It was therefore necessary to represent the wing by a lifting surface.

3.1. Shape of the Lifting Surface

The shape of the lifting surface was specified such

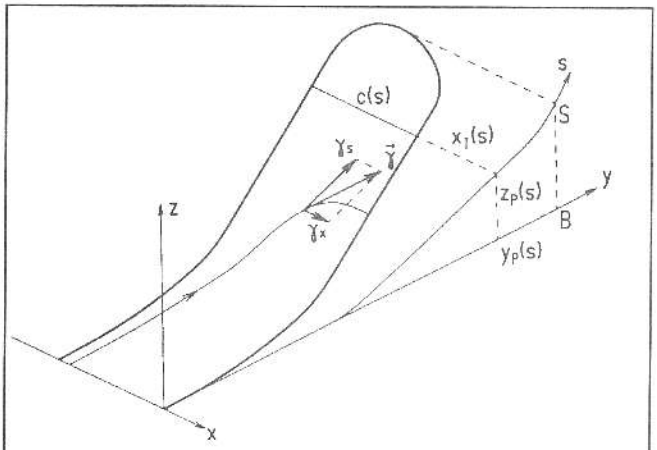

FIGURE 3.1 Definition of the wing shape.

that dihedral. vertical winglets and sweep back and sweep forward are covered. Also swept winglets are allowed. Figure 3.1 illustrates the options of the shape. The streamwise coordinate is x, the spanwise coordinate y and the vertical coordinate z. The intersections of the lifting surface with planes parallel to the x-z-plane are straight lines the projection of the lifting surface on the y-z-plane is therefore a line. This line specifies the dihedral. It is straight ($z = 0$) for a planar wing. A coordinate s is defined which is the arc length of the projection line; in the center ($y = 0$), $s = 0$. Symmetry to the x-z-plane is assumed. The projection line is defined by two functions $y_p(s), z_p(s)$. This permits inclusion of vertical winglets or even winglets which are bent more than 90°. The total length of the surface is $2S$, the half span is $\pm B = \pm y_p(S)$. For planar wings $z_p = 0$, $y_p = s$, $B = S$. The chord $c(s)$ may depend on s. Sweep back or forward is specified by the x-wise location $x_T(s)$ of the trailing edge. $x_T > 0$ means sweep back of the trailing edge, $x_T < 0$ sweep forward. In the middle $x_T = 0$ is required.

All functions $y_p(s), z_p(s), c(s)$ and $x_T(s)$ are specified so that the shape has no corners. This would cause singularities in the calculations. But small transition arcs instead of corners are allowed like those present in real wings. This is covered with good precision by the mathematical procedure.

3.2. Specification of the lift distribution

The lift distribution was pre specified. This is adequate for investigating the fundamental effect of the induced lift. The definition of the wing shape with the calculation of the lift distribution is the subject of a dissertation of J. Leyser (2). He calculates the induced forces on the wing itself for keeping the option of regarding the wake rollup. His results with respect to the induced forces are confirmed by those of the present paper.

The lift distribution is specified by the spanwise (s-wise) component γ_s of the bound vorticity. It was set

$$\gamma_s(\xi, s) = \frac{\Gamma(s)}{c(s)}\psi(\xi), \qquad \xi = \frac{x_T(s) - x}{c(s)} \tag{7}$$

with

$$\int_0^1 \psi(\xi)d\xi = 1, \qquad \psi(0) = 0 \tag{8}$$

The function $\Gamma(s)$ is circulation distribution of the wing. ξ is the normalized chordwise coordinate. At the trailing edge $x = x_T$ it is $\xi = 0$, at the leading edge : $x = x_T - c$ it is $\xi = 1$. The function $\psi(\xi)$ describes the chordwise lift distribution which is the same for all spanwise stations. It is assumed to be of the form

$$\psi(\xi) = \sum_{k=1}^{K} a_k \xi^k \tag{9}$$

A vorticity distribution $\gamma_s(\xi,s)$ does not satisfy the Helmholtz-law without a vorticity component γ_x in the x-direction. This component can be calculated by means of the Helmholtz law. At the trailing edge $\gamma_x(x_T,s) = -\Gamma(s)$. *This is the* vorticity which is continued in the wake, exactly in the same way as in the lifting line theory. A typical vortex line of the bound vorticity is sketched in Figure 3.1. In the examples of section 5 an elliptical circulation distribution

$$\Gamma(s) = \Gamma_0\sqrt{1 - \left(\frac{s}{S}\right)^2} \tag{10}$$

was mostly used. This is for nonplanar wings not the optimal circulation distribution. One example of section 5 shows, for a vertical winglet, the improvement due to a better circulation distribution which has lower Γ at the winglet. The induced drag differs not much from one with the optimal distributions. But the lower lift coefficients of the winglet allow a lower drag coefficient for the viscous correction which turns out to be more effective than the better Γ-distribution. But it is very questionable if the optimal Γ-distribution can be really achieved with a real wing. This needs a very careful design of the winglet by means of a program for the calculation of the lift distribution of a nonplanar wing of given shape. The values from the non optimal elliptical Γ-distribution are perhaps more realistic.

The difference in some way represents the fact that steep or vertical winglets can only be designed optimally for one lift coefficient. For less steep dihedral the difference is negligible.

3.3. General Results

The calculation of lift and drag is completely described in the full paper (1). Some general qualitative results can be understood without the complete mathematics.

A) Positive induced lift is present if the wake experiences negative lift. It can only be caused by velocity components toward the wing tip which are induced by the bound vorticity of the wing. Such velocity components are induced if the wing has positive dihedral or, for example, winglets above the wing tip. The opposite is true for negative dihedral and winglets below the wing tip.

B) The induced drag is correctly calculated in the Trefftz plane. It depends only on the shape of the projection line $y_p(s), z_p(s)$ and the circulation $\Gamma(s)$. The induced lift does not change those and thus the induced drag. The induced lift is therefore "free" lift with respect to the induced drag. This is a very remarkable fact. How can it be understood? Nature is normally not so generous to give something free!

The explanation is simple and clear. The velocities that the wing induces at the wake have the tendency to increase the distance between the rolled up vortices if the induced lift is positive. Without changing the circulation of these vortices, the larger distance between them is equivalent to higher span and thus to higher lift.

It is not yet proved but near at hand that the increased

distance of the rolled up wake vortices is the main effect of the rollup, and this effect is equivalent to the induced lift. This would mean that this main effect of the rollup could be calculated without really performing the adaptation of the wake to the local flow. This relaxation requires much more programming and computing effort, not only for the iterative adaptation of the wake, but also for the calculation of the forces on the wing itself, because the Trefftz plane cannot be used in this case. The old difficulties as mentioned in the introduction are then back again, and much effort in necessary to obtain at all reliable results.

The program by which the results of the present paper are computed includes an error bound and needs about 10 seconds of computing time for each case on an SPARC ELC workstation. This allows a lot of parameter variations.

C) Sweep back or forward has no effect at planar wings. This coincides with the well-known stagger theorem of Munk (5).

D) Also for nonplanar wings the effect of sweep back or forward is much smaller than the effect of dihedral. This can be seen from one example in the next section in which the sweep of vertical winglets is varied. It shows that sweep of such winglets does not pay.

E) The induced drag contains Γ in the second power whereas the lift is proportional to the first power. The induced lift is of the same order of magnitude as the induced drag. The induced lift has thus more effect at low aspect ratios and high lift coefficients. But the examples show that for high aspect ratios also the induced lift should not be neglected .

4. Representation of the Results

4.1. Effective Span

Results with respect to induced drag are normally judged by the so-called k-factor. It is defined by the equation

$$c_{d_i} = k\,\frac{c_\ell^2}{\pi\Lambda} \tag{11}$$

where c_{di} is the coefficient of the induced drag, c_l the lift coefficient and

$$\Lambda = \frac{(2B)^2}{A} \tag{12}$$

the aspect ratio of the wing. Planar wings have $k \geq 1$, only an elliptical lift distribution achieves $k = 1$. In case of nonplanar wings their area A in equation (12) can be defined in different ways. It is therefore better to rewrite equation (11) by means of the definitions of the lift and drag coefficients and to introduce an effective (half) span B^*. This is the span that a planar wing with an elliptical lift distribution and the same lift and drag would have. Using

$$D_i = q\,A\,c_{d_i} \qquad L = q\,A\,c_\ell \qquad q = \frac{\rho}{2}v_\infty^2 \tag{13}$$

where q is the dynamic pressure, it follows that

$$D_i = k\,\frac{L^2}{q\pi(2B)^2} = \frac{L^2}{q\pi(2B^*)^2} \tag{14}$$

These equations no longer contain A and, therefore, it follows that

$$B^* = \frac{B}{\sqrt{k}} = \frac{L}{\sqrt{4\pi q D_i}} \tag{15}$$

In the examples in section 5, B^* is used instead of the k-factor.

4.2. Drag Penalty from Profile Drag.

Winglets and other forms of wing tips with dihedral increase not only the effective span, but also the wetted area of the wing. Although the induced drag is considered to be completely independent of the viscous drag, for a correct comparison of different wings it is necessary to add to the induced drag that part of the viscous drag that is due to the difference in wetted areas. Two different wings 1 and 2 are to be compared. They have the effective spans B_1^* and B_2^*, the wetted areas A_1 and A_2, the lifts L_1 and L_2, and the induced drags D_1 and D_2. If for example $A_2 > A_1$, then the additional drag of wing 2

$$\Delta D = q(A_2 - A_1)c_{d_p} \tag{16}$$

must be added to the induced drag of wing 2 if it is to be compared with wing 1. Here c_{dp} is the profile-drag coefficient corresponding to the additional wing area. This is equivalent to a difference in the effective span for which from equation (15) follows

$$B_2^* + \Delta B^* = \frac{L_2}{\sqrt{4\pi q(D_2 + \Delta D)}} \tag{17}$$

This yields, if a small ΔD is assumed,

$$1 + \frac{\Delta B^*}{B_2^*} = \frac{1}{\sqrt{1 + \frac{\Delta D}{D_2}}} \approx 1 - \frac{\Delta D}{2D_2} \tag{18}$$

and, using equations (15) and (16),

$$\frac{\Delta B^*}{B_2^*} = -\frac{\pi}{2}\,\frac{(A_2 - A_1)(2B_2^*)^2}{A_2^2}\,\frac{c_{d_p}}{c_\ell^2} \tag{19}$$

In the examples in section 5 the chord distribution of the wing is elliptical with respect to the length s, which means, if c_0 is the chord at the wing root, that

$$c = c_o\sqrt{1 - \frac{s^2}{S^2}} \qquad A = 2S\,c_{av} \qquad c_{av} = \frac{\pi}{4}c_o \tag{20}$$

where c_{av} is the average chord of the wing. Assuming that the values of S, B^*, and B do not differ much it follows that

$$\frac{\Delta B^*}{B_2} \approx -\frac{4(S_2 - S_1)}{c_o}\,\frac{c_{d_p}}{c_\ell^2} \tag{21}$$

The effective span is diminished by the additional viscous drag, and c_l^2 is in the denominator of the diminish-

ing term. This may overcompensate the reduction of the induced drag if c_l is low. An example is given in section 5. It is a well known fact that winglets mainly reduce the total drag at high c_l.

4.3. Circulation and Lift Coefficient

All formulas for the induced lift always contain quadratic terms of the circulation Γ, as is true for the induced drag. This means that, the higher Γ, the greater the influence of the induced lift. It must, however, be considered that the lift coefficient of a wing section is limited. The relation between Γ and c_l can be found by expressing the local lift L by both variables, as follows.

$$L = \rho v_\infty \Gamma \, dy = \frac{\rho v_\infty^2}{2} c \, dy \qquad (22)$$

This yields

$$\Gamma = \frac{1}{2} v_\infty c \, c_\ell \qquad (23)$$

The examples in the next section, except the last one, are all calculated with $c_l = 1.5$.

5. Examples

The following examples were selected to study the effect of wing-tip shapes like winglets or short sections with dihedral on the total drag. The chordwise lift distribution is in all cases the same. In equation (9), $a_1 = 6$ and $a_2 = -6$ are used. This satisfies all the conditions that were established for ψ(ξ). Because ψ(ξ) is a parabola and symmetrical around the middle of the chord, the resulting lift is located at mid chord. The spanwise chord distribution $c(s)$ is elliptical according to equation (20). The trailing edge is straight without sweep back.

In the first example, the length $S = 1$ is constant, and 25% of S is bent up at an angle ß. This means the span becomes smaller with increasing ß. The viscous drag need not be considered because the wetted area does not change. Angles from 0 to 40° were evaluated for three aspect ratios $A = 6.4$, 12.7 and 25.5 for each ß. The results are presented in Figure 5.1. in terms of the effective span B^*.

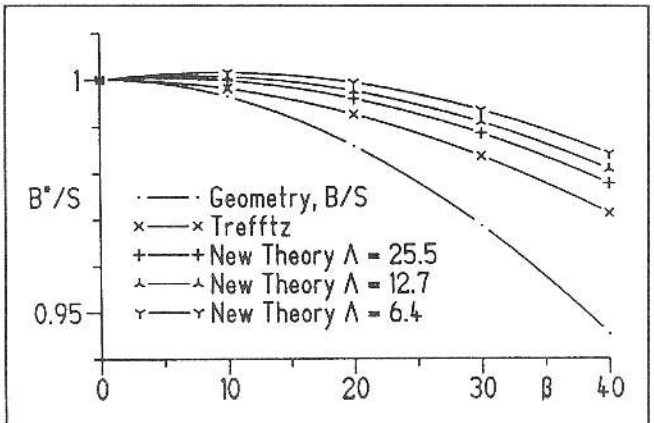

FIGURE 5.1 Effective span B^* of wings with constant length S, different aspect ratios and various dihedral angles over 25% of S.

The difference between the line labeled "Trefftz" and the line for the geometric span shows the effect of the dihedral due to the classical theory without induced lift. This theory yields exactly the same result for dihedral up and down, in this case for the same absolute value of ß but with opposite sign. This was computed to 6 significant figures. The case ß = 0 is the elliptical lift distribution for which $B^* = S$ must hold. This test was also successful to 6 figures.

The differences between the lines from the new theory and the Trefftz line show the effect of the induced lift. It depends on the aspect ratio, and it is of the same order of magnitude as the difference between the Trefftz line and the geometric span. According to the classical theory, approximately 40% of the geometric span reduction is "regained". For the low aspect ratio and low ß, the effect of the induced lift is even larger than the one of the classical theory. For all aspect ratios a wing tip with ß ≥ 10° is better than a planar wing with the same length S, and thus higher span.

The effect of the induced lift is opposite for winglets down; the lines from the new theory would be in the same distance below the Trefftz line. For low ß-values a negative dihedral near the wing tip is worse than a planar wing with the same span.

Small models with one winglet up and the other one down are capable of clearly demonstrating the effect of the induced lift.

The second example considers the fact that in many cases the span is restricted. Therefore. the wing tip is assumed at $y = B$ and $z = 0.1B$. The wing shapes range from a vertical winglet to a wing that is straight and has a small, constant dihedral from root to tip. The wetted area increases with the dihedral angle. The difference in the viscous drag is considered according to section 4.2 with $4c_{dp}/c_l^2 = 0.025$. which means for $c_l = 1.5$ $c_{dp} = 0.01406$. The results for the high aspect ratio are given in Figure 5.2.

The effective span B^* is again larger than the geometric span B. The highest B^* is achieved with the vertical

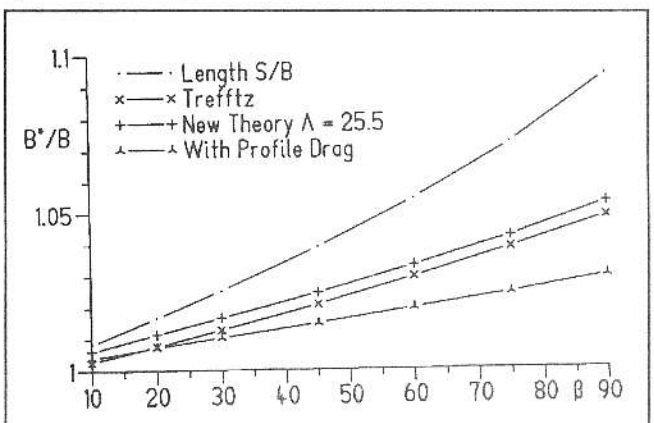

FIGURE 5.2 Effective span B^* for wings with the wing tip at $y=B=1$ and $z=0.1B$ and various dihedral angles ß. The spanwise location of the start of the dihedral depends on ß.

winglet. It is questionable however if this is in all cases the optimum. A vertical winglet does not change its geometrical angle of attack. If it is optimized for the high-lift case it yields a considerable additional induced drag at high speeds. If it is optimized for low c_l, the improvement in the high lift case is smaller. Thus, only a one point design should use a vertical winglet.

If the wing has lift increasing flaps, the multi-point problem of the vertical winglet can be reduced by extending the flap into the winglet.

The third example has the same fixed wing tip as the second one. The dihedral is now, however, assumed in the form of a circular arc instead of a corner. The results are shown in Figure 5.3. Again, only the high aspect ratio $A = 25.5$ is considered.

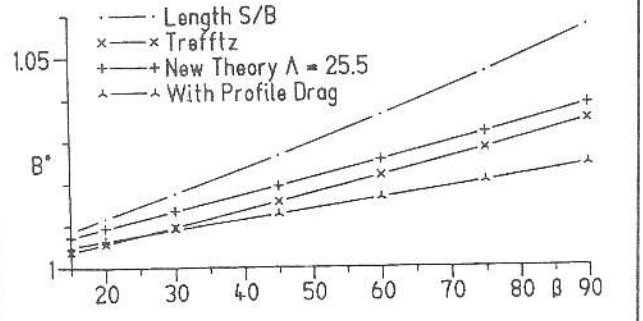

FIGURE 5.3 Effective span B* for circular arc winglets ending at a fixed wing tip position. The angle ß is the dihedral angle at the wing tip. Span $B = 1$.

The extension of the wing lengths yields now a higher increase of the effective span B^*. This is shown in more detail in Fig. 5.4.

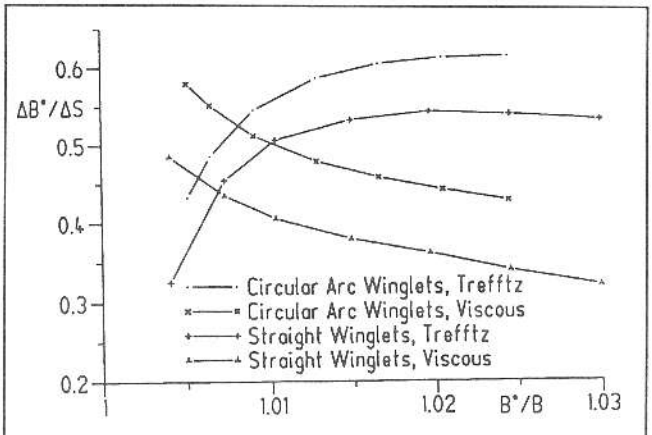

FIGURE 5.4 Relative increase $\Delta B^*/\Delta S$ against B^*/B for circular arc and straight winglets.

Fig. 5.4 shows several remarkable results:

The higher the extension $\Delta B^*/B$ of the effective span, the lower the effectivity $\Delta B^*/\Delta S$ of the length extension. This means that steep winglets are less effective than less steep ones.

Already in the Trefftz plane the circular arc winglets yield a higher increase of the effective span than the straight winglets.

The decrease of the effective span due to the profile drag is higher for the straight winglet. Altogether the circular arc winglet profits from the length extension ΔS of the wing approximately 20% more ΔB^* than the straight winglet.

It is thus better to design wing shapes that simulate the circular arc winglets, for example wings with more than one dihedral corner.

The examples given so far were calculated with $c_l = 1.5$, which is mostly realized in circling flight of gliders. The last example concerns vertical winglets of aircraft which may cruise at a lower $c_l = 0.5$. The profile drag is assumed to be $c_{dp} = 0.008$, which is a low value for a normal aircraft. The height of the winglets is varied. Figure 5.5 shows the result. The lower c_l has two effects. The induced lift is reduced because it is proportional to c_l^2 and the effect of the profile drag is much higher because it is proportional to $1/c_l^2$. This overcompensates the reduction of the induced drag due to the winglets. It is thus very questionable if the winglets of jet aircraft reduce the drag in cruise conditions, in which even lower c_l mostly occurs.

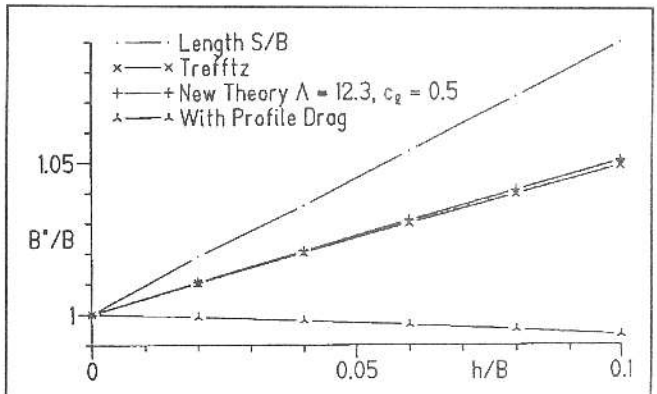

FIGURE 5.5 Effect of vertical winglets of height h.

The next example investigates the effect of the Γ-distribution for a wing with a vertical winglet. Its height is again selected as $h = 0.1B$ which means 5% of the span. The example starts from an elliptical Γ-distribution according to equation (10). Also the planform is elliptical, the aspect ratio is $A = 25.5$, $c_l = 1.5$ has again been selected. This is realized by $\Gamma_0 = 0.075$. The variation of Γ was made by reducing Γ in the winglet range in a way which approximates the optimal distribution. Near the beginning a steep droop , $\Delta\Gamma$ was introduced. The amount of the droop was between , $\Delta\Gamma = 0$ and $\Delta\Gamma = 0.003$. The last value was already beyond the optimum with respect to the induced drag, but at the winglet $c_l = 1.05$ instead of $c_l = 1.5$ for the elliptical Γ allowed a reduction of c_{dp}. This reduction was considered using $c_{dp} = 0.00625 c_l^2$. This perhaps overestimates the influence of c_l, but it shows the tendency. The results are

given in Figure 5.6. The reduction of c_{dp} is more effective than the improvement of Γ.

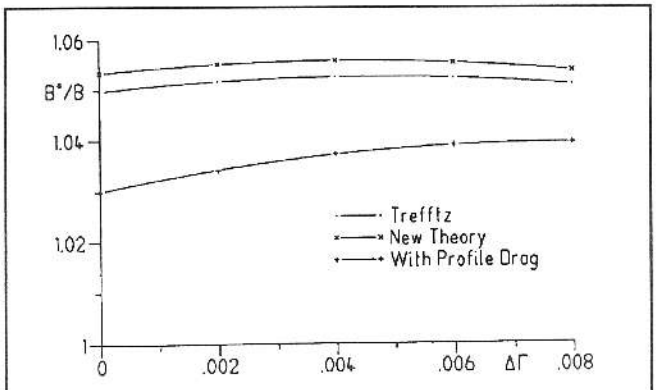

FIGURE 5.6 Effect of the improvement of Γ(s). ΔΓ is the amount of Γ-reduction at the beginning of the winglet.

The last example deals with the effect of sweep back of the winglets. The wing is the same as in the preceding example. Only the winglet is swept back by an angle ε whose tangens is the abscissa in Figure 5.7. The Γ-distribution with ΔΓ = 0.006 was used which is close to the optimum for the induced drag. The viscous correction is for all sweep angles ε the same, also the classical theory shows, of course, no effect of the sweep back. Only the induced lift has a tiny effect which probably does not justify the additional effort of the sweep back.

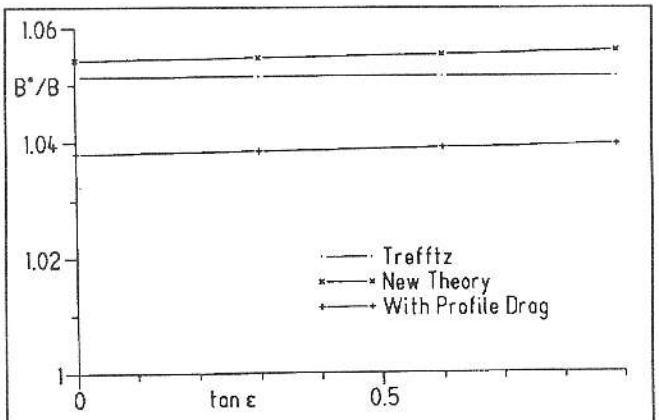

FIGURE 5.7 Effect of winglet sweep back.

Similar tiny effects have been calculated for a moderate sweep back of a total nonplanar wing.

6. Concluding Remarks, Future Work

A simple method has been presented which allows consideration of an important second order term in the theory of induced drag. This term is the induced lift, which probably is the most important effect of the wake rollup. The new theory explains the difference between positive and negative dihedral which has been demonstrated by model experiments. Many more results can be expected from this theory.

So far, the chordwise and spanwise lift distribution have been prespecified. The problem of the pre specified wing shape has been treated by J. Leyser (2). He can calculate the induced forces on the wing itself with adequate precision. He could validate his results by means of results from the present paper. His approach is the fundamental condition for regarding the complete effect of the wake rollup. So far his program requires very much computing time. The wake rollup has not yet been performed. But it seems that the computing time of his program can be reduced, and larger computers can be used to evaluate the higher order effects. This is probably the most important work to be performed in the future because it shows if really the induced lift is the prevailing higher order term as it is supposed now. If this were true, then the present theory would be subject to evaluation by means of computers which are available to anybody.

References

(1) Eppler, R.: Induced Drag and Winglets. Z. Flugwiss. u. Weltraumforschung (ZFW) 20 (1996) pp. xxxx

(2) Leyser. J.: Kraftberechnung an der nichtplanaren tragenden Fläche. Dissertation Stuttgart 1996.

(3) Maskew, B.: Prediction of Subsonic Aerodynamic Characteristics - A Case for Low-Order Panel Methods; Journal of Aircraft 19 (1982), pp. 157 -163.

(4) Multhopp, H.: Die Berechnung der Auftriebsverteilung von Tragflügeln. Luftfahrtforschung 15 (1938), pp. 153-169.

(5) Munk, M.: Isoperimetrische Aufgaben aus der Theorie des Fluges. Inaugural-Dissertation Universität Gottingen 1919.

(6) Prandtl, L.: Tragflügeltheorie. Ludwig Prandtl - Gesammelte Abhandlungen, Band 1, Berlin/ Göttingen/Heidelberg 1991, pp. 322 - 345 and pp. 377- 406.

(7) Schmid-Göller, S.: Zur genauen Berechnung des induzierten Widerstandes von Tragflügeln. Dissertation Universität Stuttgart 1992.

(8) Smith, S.C., Kroo, I.M.: A Closer Look at the Induced Drag of Crescent-Shaped Wings. AIAA-Paper 90-3063, AIAA 8th Applied Aerodynamics Conference, Portland, Oregon, August 1990.

(9) VanDam, C.P.: Induced-Drag Characteristics of Crescent-Moon-Shaped Wings; Journal of Aircraft 24 (1987), pp. 115 -119.